Energetic dysfunction and iron overload in early Parkinson's disease: Two distinct mechanisms?

Stephan Grimaldi, Arnaud Le Troter, Mohamed Mounir El Mendili, Hugo Dary, Jean-Philippe Azulay, Wafaa Zaaraoui, Jean-Philippe Ranjeva, Alexandre Eusebio, Ludovic de Rochefort, Maxime Guye

Parkinsonism and Related Disorders 124 (2024) 106996

Contents lists available at ScienceDirect

Parkinsonism and Related Disorders

journal homepage: www.elsevier.com/locate/parkreldis

Short communication

Energetic dysfunction and iron overload in early Parkinson's disease: Two distinct mechanisms?

Stephan Grimaldi [a,b,c,*], Arnaud Le Troter [b,c], Mohamed Mounir El Mendili [b,c], Hugo Dary [b,c], Jean-Philippe Azulay [a], Wafaa Zaaraoui [b,c], Jean-Philippe Ranjeva [b,c], Alexandre Eusebio [a,d], Ludovic de Rochefort [b,c], Maxime Guye [b,c]

[a] APHM, Hôpital Universitaire Timone, Department of Neurology and Movement Disorders, 264 rue Saint-Pierre, Marseille, France
[b] APHM, Hôpital Universitaire Timone, CEMEREM, 264 rue Saint-Pierre, Marseille, France
[c] Aix Marseille Univ, CRMBM, CNRS, 27 Bd Jean-Moulin, Marseille, France
[d] Aix Marseille Univ, CNRS, Institut de Neurosciences de la Timone, 27 Bd Jean-Moulin Marseille, France

ARTICLE INFO

Keywords:
Parkinson disease
Multiparametric magnetic resonance imaging
Biomarkers
Synucleinopathies
sodium

ABSTRACT

Introduction: Identifying biomarkers reflecting cellular dysfunctions in early Parkinson's disease patients (ePD) is needed to develop targeted therapeutic strategies. We aimed to determine if cellular energetic dysfunction related to increased brain sodium concentration would be co-located to microstructural alterations and iron deposition in ePD.

Methods: We prospectively included 12 ePD (mean disease duration 20.0 ± 10.2 months) and 13 healthy controls (HC), scanned with a 7 T ^{1}H and ^{23}Na MRI. Complementary voxel-based and region-based assessments were performed, the latter utilizing a high-resolution multimodal template we created (combining quantitative T_1 maps (qT1), transverse relaxation rate (R2*), quantitative magnetic susceptibility mapping (QSM) images) from 200 subjects. This template allowed a precise multiparametric assessment of sodium concentration, QSM, R_2*, qT_1, mean diffusivity, and fractional anisotropy values. A two-sided p-value<0.05 was considered statistically significant after the Bonferroni correction.

Results: Relative to HC, ePD showed significantly higher sodium concentration in left Substantia nigra (SN) pars reticulata (46.13 mM ± 3.52 vs 38.60 mM ± 6.10, $p = 0.038$), a subpart of the SN pars compacta (SNc) and ventral tegmental area, Putamen, Globus Pallidum external, accumbens nucleus and claustrum. Significantly increased QSM and R2* values, and decreased T_1 values, were limited to the Nigrosomes 1 (Nig) and right SNc (all $p < 0.05$). QSM values in the Nig were significantly correlated to UPDRS-III scores ($r = 0.91$,$p < 0.001$).

Conclusion: In ePD, brain sodium accumulation was broad and dissociated from iron accumulation. As with iron accumulation, a sodium-related pathophysiological approach could lead to identifying potential new therapeutic agents and deserves further investigation.

1. Introduction

Two pathways leading to dopaminergic neuron degeneration in Parkinson's Disease (PD) are of significant importance [1]: alpha-synuclein misfolding with Lewy bodies accumulation and mitochondrial energetic dysfunction. The latter may lead to variations in brain sodium concentration, disturbing cellular homeostasis [2]. Indeed, mitochondrial dysfunction results in ATP depletion and oxidative stress, likely exacerbating the toxic effect of the alpha-synuclein, including aggregation in an amplification loop. It also causes ubiquitin-proteasome system dysfunction, worsened by alpha-synuclein accumulation. Ultimately, a complex cascade leads to dopamine cell loss. A regulated iron-dependent cell death pathway (ferroptosis) is an additional pathophysiological process in PD, as suggested by studies linking increased brain iron levels to disease severity [3]. Enhanced levels of redox-active iron are believed to contribute to the cascade of neuronal degeneration resulting from oxidative stress. The extent to which these mechanisms are interconnected and spatially localized is unknown.

Technological and technical advances in the magnetic resonance

* Corresponding author. APHM, Hôpital Universitaire Timone, Department of Neurology and Movement Disorders, 264 rue Saint-Pierre, Marseille, France.
E-mail address: stephan.grimaldi@ap-hm.fr (S. Grimaldi).

https://doi.org/10.1016/j.parkreldis.2024.106996
Received 27 January 2024; Received in revised form 9 April 2024; Accepted 30 April 2024
Available online 6 May 2024

imaging (MRI) field have been considerable. High (3 T) and ultra-high field (7 T) brain MRI enable precise exploration and characterization of microstructural alterations in PD. These techniques highlight changes in tissue composition linked to pathophysiological processes. In the prodromal and early stages of PD, elevated quantitative maps of magnetic susceptibility (QSM) values-measuring local susceptibility and quantifying iron content in tissues-were reported in a small dopaminergic neuron-rich region within the Substantia Nigra (SN), which is compatible with the first nigrosome (Nig) and, more generally, within both the SN pars compacta (SNc) and pars reticulata (SNr) [4]. We previously reported an abnormal increase in sodium concentration in the SN in early PD subjects (ePD) in the absence of reduced volume, meaning that brain sodium accumulation may be an early marker of cellular dysfunction and neurodegeneration in PD [5]. This was possible thanks to Sodium (^{23}Na)-MRI, a cutting-edge imaging method for early disease diagnosis and treatment evaluation. It utilizes sodium ions, which are crucial for cell osmoregulation and physiology, to detect abnormalities in tissue. Healthy cells maintain sodium balance through the Na^+/K^+-ATPase pump. Disruption in energy metabolism can lead to sodium imbalance, cell dysfunction, and, ultimately, cell death.

We hypothesized that energetic dysfunction and microstructural alterations may be different but concomitant mechanisms in early PD patients (ePD). Therefore, we aimed to look at the precise location of increased brain sodium accumulation and microstructural alterations measured by T_1 relaxometry, Mean Diffusivity (MD), Fractional Anisotropy (FA), QSM, and transverse relaxation rate (R_2*) in ePD compared to healthy controls (HC) using a 7 T MRI.

2. Methods

2.1. Clinical data collection

Twelve ePD patients showing motor symptoms for less than 36 months (8 M:4 F, 55.7 ± 6.9 years-old, mean disease duration 20.0 ± 10.2 months) and 13 age-matched HC (6 M:7 F (p = 0.50), 54.0 ± 7.1 years-old (p = 0.50)) were prospectively recruited. A movement disorders specialist (SG) examined all subjects. Schwab&England (95 ± 6.7), Hoehn&Yahr (1 ± 0), and Unified Parkinson's Disease Rating Scale part III (UPDRS-III) scores (12.4 ± 3.7) confirmed mild severity. The mean levodopa equivalent dose was 182.5 ± 235.7 mg/day. Levodopa responsiveness was good for all. They had no cognitive impairment (MoCA 27.8 ± 1.7). See Table 1.

Written informed consent was obtained. Our local Ethics Committee approved the study.

2.2. MRI acquisition and data pre-processing

MRI acquisition was carried out using a Siemens Magnetom 7 T system and a 32-channel phased-array 1H head coil. The following sequences were employed.

- A sub-millimeter three-dimensional Magnetization-Prepared 2 Rapid Acquisition Gradient-Echoes (MP2RAGE) sequence.
- A transverse 3D multi-gradient echo (MGRE) sequence.
- Two sets of Diffusion-weighted (DW) spin-echo EPI sequences with 80 diffusion encoding directions (anterior-posterior (AP) and posterior-anterior (PA)) and 13 b0 volumes.

A dual-tuned 23Na/1H QED birdcage coil was used for 23Na MRI exploration, employing a multi-echo density adapted 3D projection reconstruction pulse sequence. Sodium concentration was quantified using six tubes with known concentrations (ranging from 25 to 100 mmol/L within 2% of agar gel) placed within the field of view.

MP2RAGE sequence produces a T_1-weighted (T_1-w) image (UNI) with reduced reception field bias and enables extracting a quantitative T_1 map (qT_1), corrected for the non-uniform B_1^+ excitation field, denoised and skull-stripped before registrations.

MGRE data underwent QSM reconstruction involving field inhomogeneity calculation, unwrapping, brain extraction, internal field estimation, and final MEDI reconstruction.

DW images underwent denoising and correction for Gibbs-ringing artifacts, B_1 field inhomogeneity, susceptibility, eddy currents-induced distortions, and head motion, and FA and MD maps were computed.

Sodium images were reconstructed, denoised, and motion-corrected using a multi-echo approach. Total sodium concentration (TSC) maps were estimated through bi- and mono-exponential fitting procedures.; Boundary-based registration aligned mean B0 map (FA, MD), T1w images, and sodium images using the bbregister function from *freesurfer software*. Co-registration to R2* native space was performed using the antsRegistration function with Mutual Information as a metric.

A visual quality assessment led to the exclusion of images with blurriness, significant artifacts, or unfixable registration issues. The resulting dataset for analysis included varying numbers of subjects for different imaging modalities (see Table 1).

Detailed sequence parameters and data pre-processing steps are available in the supplemental method.

2.3. Region-based segmentation

In our study, we employed a multimodal template-to-subject SyN registration using equivalent weights for QSM, R2*, and qT1 maps, enhancing accuracy and robustness to noise and artifacts. The resulting symmetrical, multiscale, and multimodal template, 7TAMIbrainqT1_R2*_QSM_400, was generated at two spatial resolutions: (1 mm)^3 for all deep gray nuclei (SN, Subthalamic nuclei (STh), RN, Putamen, Globus pallidum external (GPe), Globus pallidum internal, Caudate nucleus, Claustrum, Accumbens nucleus (Acb)) and (400 μm)^3 for specific regions (SNc, SNr, Nig, RN, STh). Two derived atlases, 7TAMIbrainDGN_*sym*_400 and 7TAMIbrainparcSN_*sym*_400, were symmetrized and resliced, facilitating the analysis of distinct brain regions.

These atlases were then warped at (600 μm)^3 in subject spaces, enabling the extraction of mean and standard deviation values for various maps (qT1, TSC, QSM, R2*, MD, FA). Further details on template construction, atlases, and SyN registration parameters can be found in the supplemental materials (Supplemental method, Supplemental Table 1, and Supplemental Fig. 1).

2.4. Voxel-based approach

The same spatial normalization (in the $7TAMIbrain_{qT1\_R2*\_QSM\_400}$ template space) was used for a voxel-wise inference employing the threshold-free cluster enhancement method (TFCE) to compare ePD and HC groups. The randomize function in the FSL toolbox was used on co-registered qT1 maps. The TFCE analysis included a Two-Sample Unpaired T-test, producing a -p-value map. Significance was considered before and after computing the family-wise error (FWE) rate, with 500 permutations and a 1 mm isotropic Gaussian smoothing applied.

2.5. Other statistical analyses

Comparisons between groups were made with Chi2 for categorical data and Wilcoxon for continuous data, as appropriate. Spearman's correlations were performed between clinical features and MRI parameters. A two-sided p-value<0.05 was considered statistically significant after the Bonferroni correction to account for multiple comparisons. Multiple regression analyses evaluated the relationship between MRI parameters (p-value<0.05).

Table 1
Participants' individual characteristics and MRI sequences considered after the quality check.

Group	age (years)	Male/ Female	Most affected body side	Bilateral parkinson signs	Disease duration (months)	LED (mg/d)	UPDRS III	Schwab & England	Hoehn & Yahr	SCOPA -AUT	Starkstein	MOCA	MRI sequences considered after the quality check				
													TSC	qT1	DWI	QSM	R2*
ePD	64	M	Left	yes	36	210	17	100	1	17	29	28	x	x	x	x	x
ePD	46	M	Left	yes	15	155	11	90	1	9	17	28	x	x	x	x	x
ePD	62	M	Right	no	26	0	15	100	1	2	24	24	x	x	x	x	x
ePD	59	M	Right	no	2	0	12	100	1	9	17	25	x	x	x	x	x
ePD	52	M	Left	no	6	100	17	100	1	9	21	30	x	x	x	x	x
ePD	53	F	Left	no	30	860	14	90	1	28	20	29	x	x		x	x
ePD	68	F	Left	yes	19	175	12	80	2	16	19	29		x		x	x
ePD	54	M	Left	no	29	250	14	90	1	9	27	29	x	x			x
ePD	49	F	Left	yes	18	260	8	90	1	14	17	29		x	x	x	x
ePD	47	F	Left	yes	18	180	11	100	1	2	12	28	x	x	x	x	x
ePD	56	M	Right	no	28	0	14	100	1	8	20	27	x	x	x	x	x
ePD	59	M	Right	no	13	0	4	100	1	4	12	28		x	x	x	x
HC	45	M	/	/	/	/	/	/	/	/	/	/	x	x	x	x	x
HC	53	M	/	/	/	/	/	/	/	/	/	/	x	x	x	x	x
HC	49	M	/	/	/	/	/	/	/	/	/	/	x	x	x	x	x
HC	52	F	/	/	/	/	/	/	/	/	/	/	x	x	x	x	x
HC	61	M	/	/	/	/	/	/	/	/	/	/	x	x	x	x	x
HC	60	F	/	/	/	/	/	/	/	/	/	/		x	x	x	x
HC	56	M	/	/	/	/	/	/	/	/	/	/	x	x	x	x	x
HC	45	F	/	/	/	/	/	/	/	/	/	/	x	x	x	x	x
HC	48	F	/	/	/	/	/	/	/	/	/	/	x	x	x	x	x
HC	52	F	/	/	/	/	/	/	/	/	/	/	x	x	x		x
HC	50	F	/	/	/	/	/	/	/	/	/	/	x	x		x	x
HC	66	F	/	/	/	/	/	/	/	/	/	/	x	x		x	x
HC	65	M	/	/	/	/	/	/	/	/	/	/	x	x	x	x	x

HC: Healthy controls; ePD: DWI: Diffusion Weighted Images; early parkinson's disease; LED: Levodopa Equivalent dose; R2*: transverse relaxation rate; QSM: quantitative maps of magnetic susceptibility; qT1: quantitative T1; TSC: Total sodium concentration.
x: image considered in the analyses.

3. Results

3.1. Region-based analysis

In the 7TAMIbrainDGN_*sym*_400 atlas, ePD showed significantly higher TSC in the SN, putamen, GPe, claustrum and Acb. No significant difference was found between HC and ePD nor in QSM, R_2*, T_1 in MD or FA values. See Supplemental Fig. 2 and Supplemental Table 2.

In the midbrain exploration (7TAMIbrainparcSN_*sym*_400 atlas), ePD exhibited higher TSC in the left SNr, increased QSM values in the left and right Nig, and decreased qT1 values in the left Nig and right SNc. No significant differences were found in DWI parameters between groups. See Supplemental Fig. 3 and Supplemental Table 3.

Multiple regression analyses showed that subjects with higher TSC values in the left SNr ($F(2,14) = 5.24$, adjusted $R^2 = 0.35$,$p = 0.02$) were expected to have lower MD ($t = -3.04$,$p = 0.0088$) and higher qT1 values ($t = 2.88$,$p = 0.0121$). Those with higher TSC values in the claustrum ($F(4,11) = 4.78$, adjusted $R^2 = 0.50$,$p = 0.0176$) were expected to have lower MD values ($t = -2.91$,$p = 0.0143$). Those with higher QSM values in the Nig were expected to have lower FA values (left: $F(5,1) = 317.18$, adjusted $R^2 = 0.99$,$p = 0.04$; $t = -30.87$,$p = 0.0206$; right: $F(2,16) = 24.71$, adjusted $R^2 = 0.72$,$p < 0.0001$; $t = -2.20$,$p = 0.0432$).

3.2. Voxel-based analysis

Voxel-based analysis around the midbrain revealed higher TSC in ePD within the left SNc, SNr, and ventral tegmental area (VTA) ($p < 0.05$ FWE corrected). Additionally, increased FA and decreased MD were observed in the left VTA and surrounding white matter fibers ($p < 0.05$ FWE corrected).

QSM values tended to be higher, while qT1 values tended to be lower in ePD within the Nig and part of the SNc. R2* showed tendencies of elevation in overlapping areas (QSM, qT1, and R2*$p < 0.05$, FWE uncorrected). See Fig. 1.

3.3. Correlations with clinical features

QSM and R2* values within the Nig (left + right) were positively correlated with the UPDRS-III motor score (see Supplemental Fig. 4). No correlation was found between TSC values and UPDRS-III total or subparts (left vs right).

4. Discussion

In this 7 T MRI study of ePD, we identified significant sodium homeostasis dysfunction, which simultaneously affected the sub-cortical and brainstem structures (putamen, Gpe, claustrum, Acb, SN, STh, VTA) whereas iron overload (elevated QSM, R2* values) was mainly limited to the Nig, although it affected the right SNc more widely. MD and FA changes revealed the involvement of another subpart of VTA.

These results suggest distinct but concomitant neurodegenerative pathways in the early stage of PD.

4.1. A wide brain sodium accumulation

After less than three years with motor symptoms, brain sodium accumulation was already widespread, which might be related to mitochondrial energetic dysfunction. Physiologically, changes in mitochondrial gene expression, well-documented in the SN [6], contribute to cellular energy failure, which in turn leads to loss of function of Na^+/K^+ ATPase and impaired ability of the cell to maintain resting potential and to export Na^+ [2]. Also, mitochondrial dysfunction may result in intraneuronal sodium overload through reversed activity of the sodium-calcium exchanger and axonal calcium import [2]. This pathophysiological process could lead to the identification of new therapeutic targets, such as the $Na^+K^+Cl^-$ cotransporter isoform 1 (NKCC1) importer antagonist, which has been reported to have a neuroprotective effect in PD through its action on astrocytes, microglia, and oligodendrocytes by limiting the intracellular accumulation of NA^+, Cl^- and K^+ [7].

Also, sodium accumulation occurred in the STh, putamen, and GPe. It is well-known that dysfunction of the SNc leads to inadequate modulation of the activity of neurons in the basal ganglia. In the end,

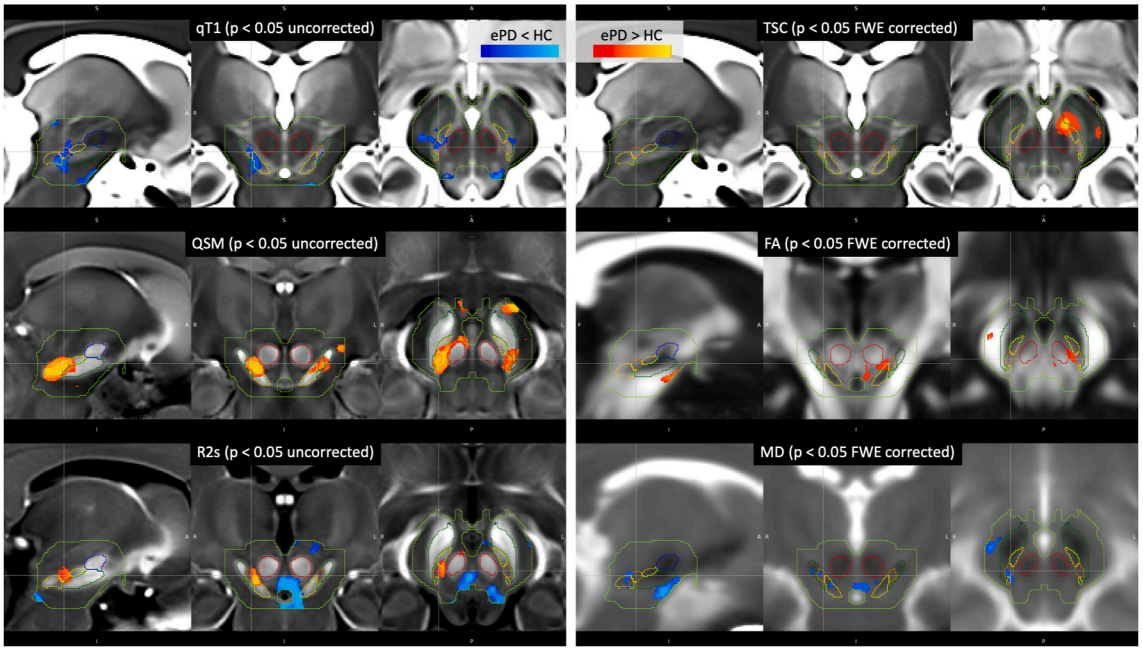

Fig. 1. P-values maps resulting from voxel-based analysis for each map (qT1,R2*,QSM, TSC,FA, and MD) on sagittal, coronal, and axial views, superposed on the $7TAMIbrain_{qT1\_R2*\_QSM\_400}$ template (analysis restricted to the midbrain at (400 μm)^3 inside the region delimitated in light green). Dark Green: Substantia Nigra pars reticulata (SNr); Orange: nigrosome; Red: Red nucleus; Yellow: Substantia Nigra pars compacta (SNc)

inadequate facilitation of the corticospinal tracts produces akinesia and bradykinesia, which are part of the Parkinsonian syndrome. Besides, sodium accumulation occurred in the VTA and Acb. Dopaminergic inputs from the VTA modulate the Acb. Thus, the VTA participates in reward consumption and addiction behaviors and regulates learning/memory functions. Nevertheless, the high VTA impairment variability reported in the literature may explain the heterogeneity of PD non-motor symptoms [8], and the early vs. delayed onset of symptoms. Finally, sodium accumulation was also found in the claustrum, an understudied structure that was reported to be connected to neocortical areas such as the frontal cortex, visual cortical fields, temporal cortex, entorhinal cortex, parieto-occipital cortex, and to basal ganglia. Further investigation would be necessary to determine its involvement in non-motor symptoms.

The absence of correlations between sodium accumulation and clinical scores hinders direct linkage between our patients' symptoms and these biomarker abnormalities. Clinically, the most affected body side was left in 8/12 (with 5 where bilateral involvement was noticed) and right in 4/12 (0 with bilateral involvement) subjects. Thus, the left SN would be expected to be affected in 8/12 subjects (67%) and the right SN in 9/12 (75%) subjects. Although non-statistically significant, sodium accumulation was also noticed in the right SN. Ultimately, this bilateral involvement may reduce the sodium burden differences between the left and right SN, resulting in a nonsignificant correlation with the UPDRS-III total (and subparts -left and right-scores). Nonetheless, those subclinical biochemical modifications might worsen over time or disease severity. In 10 severe patients with Progressive Supranuclear Palsy (PSP), increased sodium concentration in the left midbrain correlated with the PSP rating scale but not the UPDRS-III [9]. Further investigations and follow-up studies are needed to address this assumption.

4.2. A limited iron accumulation

Our results align with studies in which QSM values were reported to be higher in SN and reflect the levodopa dosage and disease severity [3]. Precisely, iron overload was mainly limited to the Nig. Iron storage's spatial distribution within SN matches dopaminergic neuron loss, suggesting a relationship between the two processes. The ventrolateral tier of the SNc, which corresponds to the Nig, is the first region affected by neuronal loss and the most affected throughout the disease.

Iron plays an essential role in several biological processes in the brain. Histochemical studies reported increased iron levels (primarily ferritin-iron and neuromelanin-iron load) in the SN of PD patients. In normal brains, there are high levels of basal oxidative stress in the SN, and this phenomenon is primarily increased in PD. Indeed, dopamine metabolism impairment might be responsible for the high level of basal oxidative stress in the SN. Then, oxidative stress is thought to contribute to the cascade of neuronal degeneration resulting from enhanced levels of redox-active iron. Consequently, increased brain iron may lead to a vicious cycle of oxidative stress by increasing free iron levels. This process involves the release of iron from ferritin, heme proteins, and iron-sulfur proteins [10].

No relationship between sodium and iron accumulation was found. This result, along with the discrepancy of the regions involved in those pathophysiological pathways, may suggest different but concomitant neurodegenerative processes in ePD.

4.3. Other microstructural changes and sodium/iron relationship

Variations in qT1 are consistent with previous reports, although they considered the global SN [11]. Those variations have been interpreted as being related to either a change in the lattice and cell density or a change in water binding, free iron, and neuromelanin burden.

MD and FA reported values in the literature are heterogeneous and probably dependent on disease stage, regions assessed, and dopaminergic state [12]. Here, sodium accumulation, along with lower MD values in the left SNr and claustrum, may suggest cell swelling before death or cellular proliferation to compensate for neurodegeneration. Further studies are necessary to estimate where the sodium accumulation occurs (e.g., intra- or extracellular space) with the help of different new MRI techniques (such as an inversion recovery ^{23}Na protocols and an evaluation of the $T_2{}^*_{short}$ and $T_2{}^*_{long}$ Na signal components).

In the Nig, higher QSM values were related to lower FA, and were concomitant with lower qT1 values. Those results are compatible with loss of microstructural integrity and increased iron burden.

Finally, higher FA and lower MD values may suggest selective neurodegeneration or compensatory neuroplasticity in the VTA. Creating a VTA sub-nuclei atlas at 7 T could enhance our understanding of its changes.

4.4. Limits

The primary limitation is the constrained participant number due to the replacement of the 7 T scanner, halting further enrollment. However, leveraging ultra-high field MRI for signal acquisition optimization, rigorous quality checks, and the use of an optimized atlas in both region-based and voxel-based analyses allowed us to uncover significant group differences despite this limitation.

Also, no motor or cognitive assessment was performed in the HC group. Nevertheless, the movement disorder specialist (SG) observed no evidence of parkinsonism or cognitive slowness before they performed the MRI.

Finally, no clinical correlation was found between sodium accumulation and clinical scores, probably because of the limited number of subjects and the mild motor impairment in the subjects.

5. Conclusion

This multiparametric and multiscale quantitative analysis at 7 T provided new insights into the pathophysiological process of neurodegeneration in the early stage of PD. Brain sodium accumulation (reflecting mitochondrial energetic dysfunction) was broad, affecting subcortical and brainstem structures, and dissociated from iron accumulation which was limited to the bilateral Nig and the right SNc. Just as with iron accumulation, a sodium-related pathophysiological approach could lead to identifying potential new therapeutic agents. Further investigation is ongoing.

Funding sources for the study

This work was supported by ANR (ANR-15-CE19-0019-01, 'NEUROintraSOD-7T') and A*MIDEX (A*MIDEX-EI-17-29-170228-09.43-Imetionic-7, 7TEAMS Chair). Also, this work was performed by a laboratory member of the France Life Imaging network (grant ANR-11-INBS-0006).

Data and code availability statement

The full multimodal 7TMarsPark dataset (BIDS formatted) containing all contrasts and atlases maps cropped around the SN region (for full disidentification) is available on demand by contacting the corresponding author.. Singularity and docker containers for Python source code, registration, and atlas-based segmentation can be found in the GitHub repository at https://github.com/arnaudletroter/7TAMI_MM.git

CRediT authorship contribution statement

Stephan Grimaldi: Writing – review & editing, Writing – original draft, Visualization, Methodology, Investigation, Formal analysis, Data

curation, Conceptualization. **Arnaud Le Troter:** Writing – review & editing, Writing – original draft, Visualization, Software, Methodology. **Mohamed Mounir El Mendili:** Writing – review & editing, Visualization, Formal analysis, Data curation. **Hugo Dary:** Writing – review & editing, Writing – original draft, Software, Methodology, Formal analysis, Data curation. **Jean-Philippe Azulay:** Writing – review & editing, Supervision. **Wafaa Zaaraoui:** Writing – review & editing, Validation, Supervision, Resources. **Jean-Philippe Ranjeva:** Writing – review & editing, Validation, Supervision. **Alexandre Eusebio:** Writing – review & editing, Validation, Supervision, Conceptualization. **Ludovic de Rochefort:** Writing – review & editing, Writing – original draft, Software, Methodology, Formal analysis, Data curation. **Maxime Guye:** Writing – review & editing, Validation, Supervision, Project administration, Conceptualization.

Declaration of competing interest

No COI.

Appendix A. Supplementary data

Supplementary data to this article can be found online at https://doi.org/10.1016/j.parkreldis.2024.106996.

References

[1] P.M. Abou-Sleiman, M.M.K. Muqit, N.W. Wood, Expanding insights of mitochondrial dysfunction in Parkinson's disease, Nat. Rev. Neurosci. 7 (2006) 207–219, https://doi.org/10.1038/nrn1868.

[2] S.G. Waxman, Axonal conduction and injury in multiple sclerosis: the role of sodium channels, Nat. Rev. Neurosci. 7 (2006) 932–941, https://doi.org/10.1038/nrn2023.

[3] V. Shahmaei, F. Faeghi, A. Mohammadbeigi, H. Hashemi, F. Ashrafi, Evaluation of iron deposition in brain basal ganglia of patients with Parkinson's disease using quantitative susceptibility mapping, European Journal of Radiology Open 6 (2019) 169–174, https://doi.org/10.1016/j.ejro.2019.04.005.

[4] S. Lehéricy, E. Bardinet, C. Poupon, M. Vidailhet, C. François, 7 tesla magnetic resonance imaging: a closer look at substantia nigra anatomy in Parkinson's disease: 7T MRI in PD, Mov. Disord. 29 (2014) 1574–1581, https://doi.org/10.1002/mds.26043.

[5] S. Grimaldi, M.M. El Mendili, W. Zaaraoui, J.-P. Ranjeva, J.-P. Azulay, A. Eusebio, M. Guye, Increased sodium concentration in substantia nigra in early Parkinson's disease: a Preliminary study with ultra-high field (7T) MRI, Front. Neurol. 12 (2021) 715618, https://doi.org/10.3389/fneur.2021.715618.

[6] C. Dölle, I. Flønes, G.S. Nido, H. Miletic, N. Osuagwu, S. Kristoffersen, P.K. Lilleng, J.P. Larsen, O.-B. Tysnes, K. Haugarvoll, L.A. Bindoff, C. Tzoulis, Defective mitochondrial DNA homeostasis in the substantia nigra in Parkinson disease, Nat. Commun. 7 (2016) 13548, https://doi.org/10.1038/ncomms13548.

[7] F. Boscia, G. Begum, G. Pignataro, R. Sirabella, O. Cuomo, A. Casamassa, D. Sun, L. Annunziato, Glial Na^+-dependent ion transporters in pathophysiological conditions: Glial Na^+-dependent Transporters in CNS Diseases, Glia 64 (2016) 1677–1697, https://doi.org/10.1002/glia.23030.

[8] A. Hassan, E.E. Benarroch, Heterogeneity of the midbrain dopamine system: implications for Parkinson disease, Neurology 85 (2015) 1795–1805, https://doi.org/10.1212/WNL.0000000000002137.

[9] J. Prasuhn, M. Göttlich, S.S. Großer, K. Reuther, B. Ebeling, C. Bodemann, H. Hanssen, A.M. Nagel, N. Brüggemann, Increased subcortical sodium levels in patients with Progressive Supranuclear Palsy, Biomedicines 10 (2022) 1728, https://doi.org/10.3390/biomedicines10071728.

[10] D.W. Reif, Ferritin as a source of iron for oxidative damage, Free Radic. Biol. Med. 12 (1992) 417–427, https://doi.org/10.1016/0891-5849(92)90091-T.

[11] R.A. Menke, S. Jbabdi, K.L. Miller, P.M. Matthews, M. Zarei, Connectivity-based segmentation of the substantia nigra in human and its implications in Parkinson's disease, Neuroimage 52 (2010) 1175–1180, https://doi.org/10.1016/j.neuroimage.2010.05.086.

[12] X.-Y. Deng, L. Wang, T.-T. Yang, R. Li, G. Yu, A meta-analysis of diffusion tensor imaging of substantia nigra in patients with Parkinson's disease, Sci. Rep. 8 (2018) 2941, https://doi.org/10.1038/s41598-018-20076-y.